Biological Evaluation, Chelation, and Molecular Modeling Studies of Novel Metal-Chelating Inhibitors of NF-κB-DNA Binding: Structure Activity Relationships

Rakesh K. Sharma,*[,†] Shilpa Chopra,[†] Som D. Sharma,[†] Vineet Pande,[‡] Maria J. Ramos,[‡] Kazuyuki Meguro,[§] Jun-ichiro Inoue,[§] and Masami Otsuka[||]

Department of Chemistry, University of Delhi, Delhi-7, India, REQUIMTE/Departamento de Química, Faculdade de Ciências, Universidade do Porto, Rua do Campo Alegre 687, 4169-007 Porto, Portugal, Institute of Medical Science, University of Tokyo, Shirokane-dai, Minato-ku, Tokyo 108-0071, Japan, and Faculty of Medical and Pharmaceutical Sciences, Kumamoto University, 5−1 Oe-honmachi, Kumamoto 862-0973, Japan

Received June 29, 2005

Previously, we have reported that aurintricarboxylic acid (ATA) is one of the most potent inhibitors of the DNA binding of transcription factor NF-κB. We now report the NF-κB-DNA binding inhibitory activity of ATA analogues. An electrophoretic mobility shift assay has shown that bromopyrogallol red (BPR) is the most effective inhibitor of NF-κB-DNA binding among the studied analogues. The molecular modeling studies showed that BPR makes a strong network of hydrogen bonds with the DNA-binding region of the p50 subunit of NF-κB and has electronegative potential on its peripheral surface. Because zinc has been reported to influence the DNA binding of NF-κB, the interaction of these analogues with zinc was studied. Chemical speciation and formation-constant studies showed that BPR forms the most stable 1:1 complex with zinc. BPR has also been found to be the most potent antioxidant among the studied analogues.

Introduction

The replicative cycle of HIV comprises a number of steps that could be considered adequate targets for chemotherapeutic intervention.[1] Most of the HIV inhibitors have shown problems, such as poor absorption and bioavailability, less antiviral specificity, and failure due to mutations in the virus. The frequently observed mutation of HIV-1 is known to be a cause of drug resistance. Thus, there is a clear need for new antiviral agents that affect unique targets that are not subject to mutations. One such novel target is the host cell's transcription factor, nuclear factor-kappa B (NF-κB), which plays an important role in the regulation of HIV-1 gene expression. Targeting NF-κB evades the problem of resistance because it is a normal part of the T-cell and is not subject to mutation.

NF-κB belongs to a family of transcription factors (Rel/NF-κB) that are sequestered in the cytoplasm by specific IκB proteins.[2−7] NF-κB can exist in homo or heterodimeric forms. In the case of HIV-1, the predominant NF-κB complex in the T-cells is the p50−p65 heterodimer.[8] NF-κB binds to the target DNA (κB sites), and initiates gene expression.[9,10] Recent studies have shown that the p50 subunit of the NF-κB complex is the one that mainly interacts with the HIV-1 long-terminal repeat (LTR).[11,12] The LTR κB site contains the sequence 5′-GG-GACTTTCC-3′. The specific amino acids that are responsible for the interaction with the DNA are residues 59−71 of the p50 subunit (59: Arg, Tyr, Val, Cys, Glu, Gly, Pro, Ser, His, Gly, Gly, Leu, Pro: 71).[13,14]

It is the viral gene expression, where NF-κB plays a crucial role by binding to the HIV LTR reporter sequence (the κB site).[6,15] Biochemical studies have shown a correlation between the activation of NF-κB and the transcription of HIV-LTR.[6,15,16] The strong dependence of HIV gene expression on NF-κB has made it an important and potential drug target. The drugs studied against NF-κB fall mainly into three categories:[17] antioxidants against oxidative stress conditions, which aid in NF-κB activation; IκB phosphorylation and degradation inhibitors; and NF-κB-DNA binding inhibitors. We have mainly studied NF-κB-DNA binding inhibitors that prevent free NF-κB from binding to DNA.[18−22] These include histidine−pyridine metal chelators and aurintricarboxylic acid (ATA), the latter being one of the strongest inhibitors of NF-κB-DNA binding among the molecules tested so far.[22] This prompted us to undertake the present study, wherein we investigate the NF-κB-DNA binding inhibitory activity of ATA analogues with the aim of establishing a structure−activity relationship.

According to current estimates, over 2000 transcription factors are zinc-dependent.[23] Several studies have been done to investigate the zinc-dependent mechanism of the DNA binding of NF-κB.[19,22,24] All of these studies with respect to recombinant NF-κB-p50 binding to DNA suggest that NF-κB recognizes DNA by using zinc-dependent motifs, and zinc may also play a role in cross-linking the DNA binding of the p50 dimer.[24] Therefore, considering the possible zinc binding of these ATA analogues, we have studied the effect of Zn^{2+} on the inhibitory activity of the most potent inhibitors and have also determined the formation constant of the zinc complexes of these analogues.

Results and Discussion

ATA analogues pyrocatechol violet (PV), aurin(AU), pyrogallol red (PR), bromopyrogallol red (BPR), fluorescein (FL), chrome azurol S (CAS), and eriochrome cyanine R (ECR) were used in the present study. The structures of the analogues are indicated in Figure 1. Figures 2−4 show the inhibitory effect of these analogues on the DNA binding of $(p50)_2$ at 30 and 100 μM concentrations as demonstrated by the electrophoretic mobility shift assay (EMSA). It was carried out by using the chemiluminescence method, which offers the sensitivity and speed without producing hazardous radioactive waste. ATA analogues BPR and PR were found to exhibit remarkable inhibitory effects on the DNA binding of $(p50)_2$, both at 30

* Corresponding author. Tel: +91-11-27666250. Fax: +91-11-27666250. E-mail: rksharma@vsnl.com.
† University of Delhi.
‡ Universidade do Porto.
§ University of Tokyo.
|| Kumamoto University.

10.1021/jm050617x CCC: $33.50
Published on Web 05/16/2006

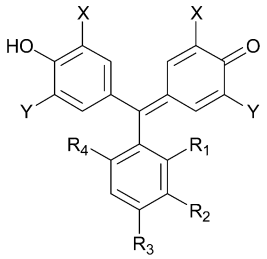

	X	Y	R_1	R_2	R_3	R_4
Aurintricarboxylic acid (ATA)	COOH	H	H	COOH	OH	H
Pyrocatechol Violet (PV)	OH	H	SO_3H	H	H	H
Aurin (AU)	H	H	H	H	OH	H
Chrome Azurol S (CAS)	COONa	CH_3	Cl	SO_3Na	H	Cl
Eriochrome Cyanine R (ECR)	COONa	CH_3	SO_3Na	H	H	H

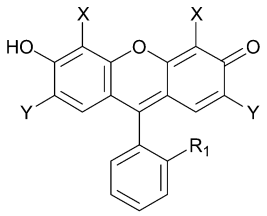

	X	Y	R_1
Pyrogallol Red (PR)	OH	H	SO_3H
Bromopyrogallol Red (BPR)	OH	Br	SO_3H
Fluorescein (FL)	H	H	COOH

Figure 1. Structures of ATA analogues.

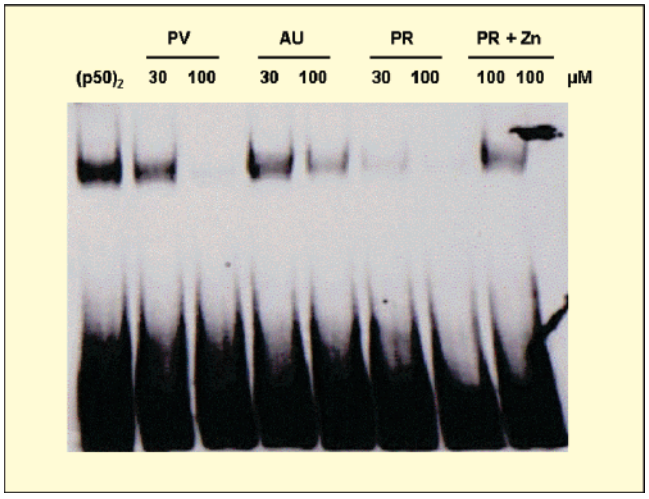

Figure 2. Effects of pyrocatechol violet (PV), aurin (AU), pyrogallol red (PR) on the DNA binding of $(p50)_2$. The effect of zinc on the inhibition of the DNA binding of $(p50)_2$ by PR is also shown.

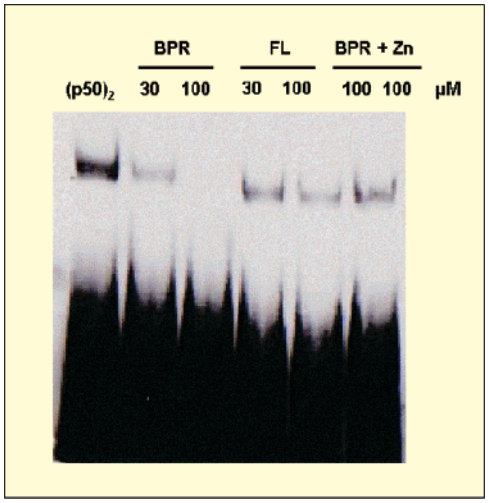

Figure 3. Effect of bromopyrogallol red (BPR) and fluorescein (FL) on the DNA binding of $(p50)_2$. The effect of zinc on the inhibition of the DNA binding of $(p50)_2$ by BPR is also shown.

and 100 μM concentrations, whereas PV was effective at 100 μM. FL, CAS, ECR, and AU did not show significant inhibitory effects at both concentrations. The most potent one was BPR, which inhibited DNA binding almost completely at 30 μM concentration, suggesting the IC_{50} value of micromolar order.

Several studies have demonstrated that zinc influences the DNA binding of NF-κB. Zabel et al.[19] have showed that the binding of NF-κB to DNA was specifically blocked by the chelating agent 1,10-orthophenanthroline and could be reconstituted only by the addition of zinc. Otsuka et al.[20] have examined the effects of four novel heterocyclic chelator compounds comprising (dimethylamino) pyridine and histidine units and their zinc complexes on NF-κB binding to DNA. Sharma et al.[22] demonstrated that ATA inhibited NF-κB-DNA binding at a very low concentration and that the addition of zinc(II) partially restored the DNA binding property of NF-κB. Prasad et al.[24] have suggested that NF-κB recognizes DNA by using zinc-dependent motifs. Zinc may also play a role in cross-linking the DNA binding of the p50 dimer. Hence, the zinc-binding behavior of these analogues may be correlated with their ability to inhibit NF-κB-DNA binding. The zinc affinity of the analogues PV, PR, BPR, CAS, and ECR was studied pH-metrically. The formation constants for the zinc complexes of these dyes were calculated using the pH measurement method of Bjerrum,[25] as modified by Irving and Rossotti.[26] The values were refined using the weighted least-squares method and are given in Table 1 along with the values of the protonation constants for the analogues. The order of the stability constants

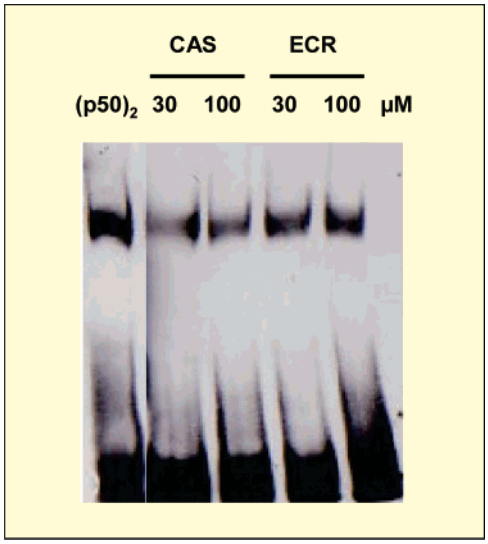

Figure 4. Effect of chrome azurol S (CAS) and eriochrome cyanine R (ECR) on the DNA binding of $(p50)_2$.

Table 1. Overall Equilibrium Constants for Zn^{2+}−ATA Analogue Complexes

ATA analogue	log β_{HL}	log β_{H2L}	log β_{H3L}	log β_{H4L}	log β_{ML}	σ_{fit}
pyrocatechol violet	11.34	20.34	25.42		7.48	0.06409
pyrogallol red	11.39	22.08	29.66	32.91	7.88	0.27948
bromopyrogallol red	11.10	21.60	28.06	31.66	9.71	0.01405
chrome azurol S	11.62				5.88	0.42193E-11
eriochrome cyanine R	11.32				5.95	0.15259E-07

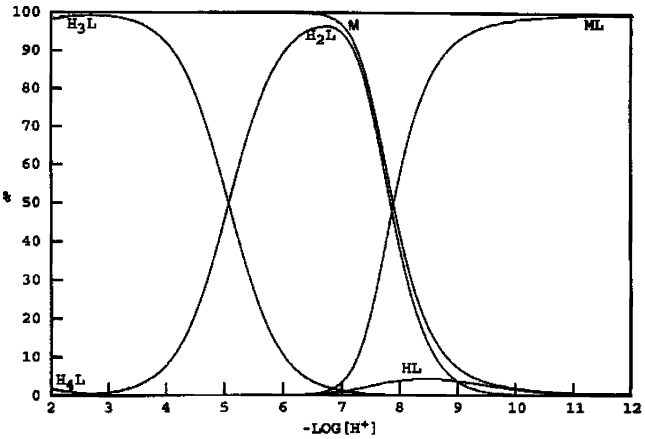

Figure 5. Species distribution curve of PV−Zn (II). Total ligand concentration, T_L (PV) = 2.50×10^{-3} M; total metal concentration, T_M (Zn(II)) = 2.50×10^{-3} M; ionic strength, μ = 0.1 M ($NaClO_4$); temperature, T = 25 °C (± 0.5°C).

for the zinc complexes are BPR > PR > PV > ECR > CAS, which is the same as those obtained from EMSA results. The species distribution curves for the zinc complexes for PV, PR, and BPR were drawn using the program SPE[27] and are shown in Figures 5−7.

The EMSA experiments were also done with zinc (one equivalent) being introduced after the DNA-binding inhibition reaction with BPR (Figure 3, column 6). A partial recovery of the $(p50)_2$−DNA complex was observed. Similar results were also obtained for PR (Figure 2, column 8). This provides additional support for the zinc-dependent mechanism of NF-κB-DNA binding. The reversal of inhibition by the addition of zinc could be accounted for by invoking the zinc chelate formation of the inhibitor.

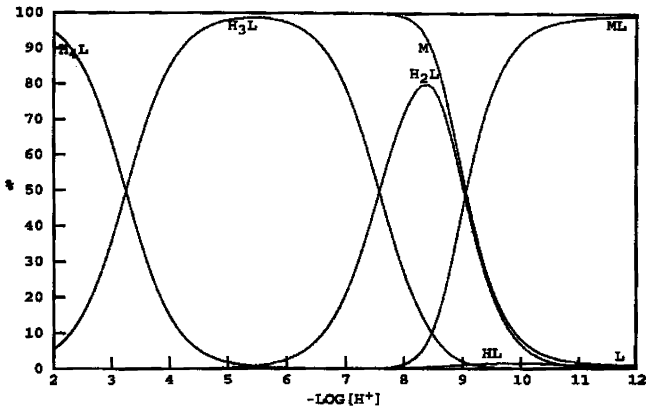

Figure 6. Species distribution curve of PR−Zn (II). Total ligand concentration, T_L (PR) = 2.53×10^{-4} M; total metal concentration, T_M (Zn(II)) = 2.53×10^{-4}M; ionic strength, μ = 0.1 M ($NaClO_4$); temperature, T = 25 °C (± 0.5 °C).

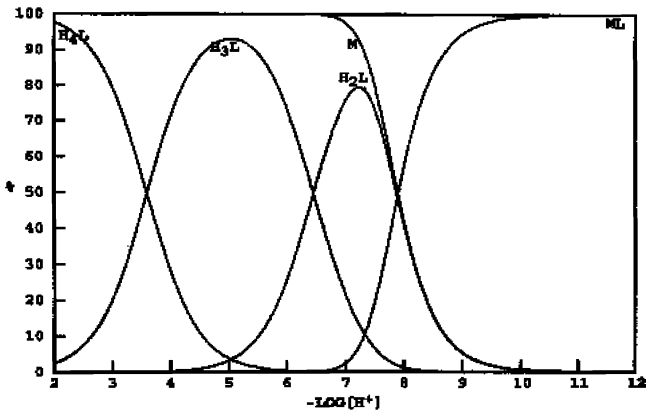

Figure 7. Species distribution curve of BPR−Zn (II). Total ligand concentration, T_L (BPR) = 2.53×10^{-4} M; total metal concentration, T_M (Zn(II)) = 2.53×10^{-4} M; ionic strength, μ = 0.1 M ($NaClO_4$); temperature, T = 25 °C (± 0.5°C).

In an effort to rationalize the results obtained from EMSA studies, we resorted to the application of molecular modeling and computational methods with the intention of analyzing and reviewing the structure of the DNA-binding region (DBR) in complex with the analogue and explaining the structure−activity relationships observed within this class. Biochemical studies have hinted at a relationship between the structural conformation of p50 with its DNA binding ability and function.[8] It is plausible that the analogues that have stronger interactions with important amino acid residues such as Ser66, His67, and Arg59 of the DBR of p50 would affect its conformation the most, thereby acting as good NF-κB-DNA binding inhibitors.[21,28] Considering this, the analogues were docked to the DBR (amino acid residues 59−71) of NF-κB (p50). The docked complexes were refined with a progressive energy-minimization protocol using the AMBER force field. Figures 8 and 9 depict the interaction of the analogues with the p50-DNA binding region after energy refinement. It is clear from these docked complexes that BPR, PR, and PV which are active can form extensive hydrogen bonds with the DBR of p50 than AU, CAS, ECR, FL, which are inactive and make only weak interactions. Additionally, BPR has two bromine groups, which provide it with the ability to fit better and deeper in the DBR because of good van der Waals interactions. In addition, molecular electrostatic potential (MEP) maps were generated for each analogue after its geometry was energy-minimized (Supporting Information). The study of such potential maps provides insight in understanding the nature of molecular recognition in bimolecular association.[29] Theoretically

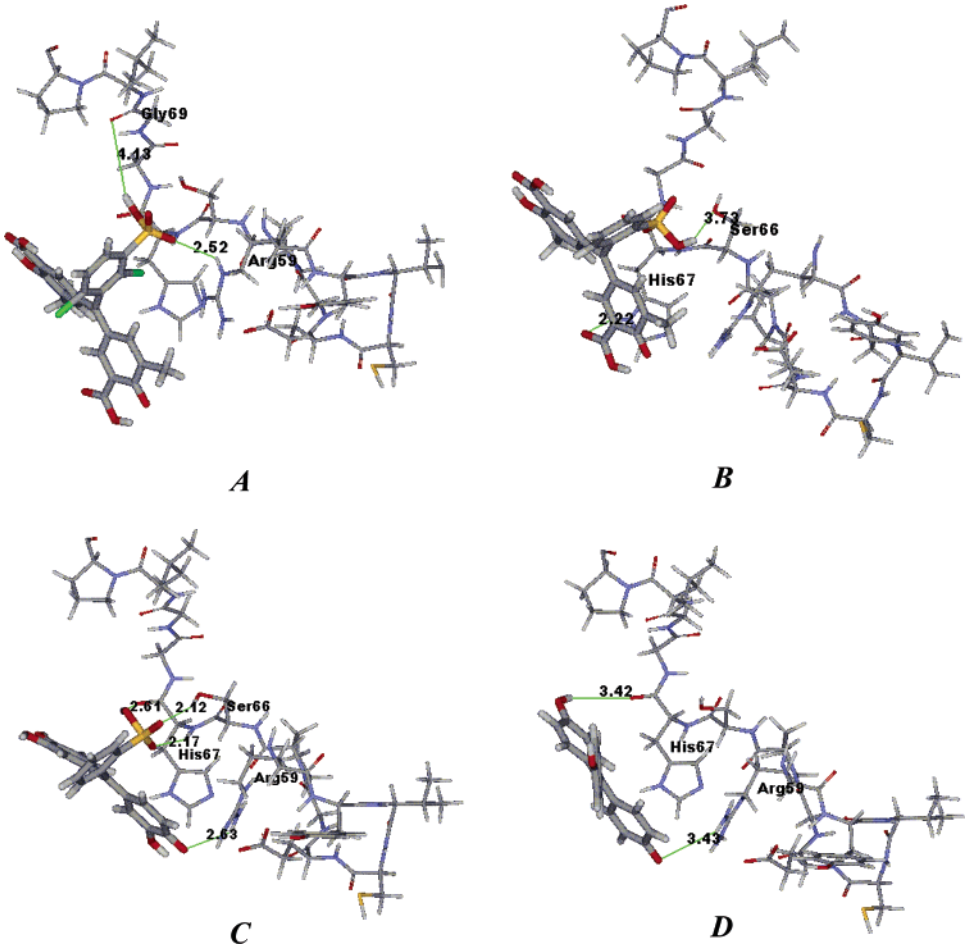

Figure 8. Possible binding modes of the ATA analogues with the p50 DNA binding region. A−D represent the complexes with analogues CAS, ECR, PV, and AU, respectively. The hydrogen bonds are depicted as green lines, and the distances are in Å.

calculated potentials, using ab initio methods, have been described to be very predictive.[18,28] A comparison of the MEPs reveals that better inhibitors such as BPR have a net electronegative potential around them. In a previous study of several different classes of NF-κB (p50)-DNA binding inhibitors, it has been found that the p50-DBR is rendered in a net electropositive potential[28] and that the better inhibitors are the ones that have relatively more electronegative MEP surfaces. Similarly, in the present case, inhibitors such as BPR also show better binding characteristics, on the basis of the complementarity of electrostatics with the DBR. Further, BPR and PR have been found to form stronger complexes with zinc on the basis of their greater ability to complex with positively charged metal because of the presence of more electronegative potentials on their surfaces.

It has been shown that antioxidants inhibit NF-κB-mediated transcriptional activation because reactive oxygen species are known to stimulate NF-κB activation.[17] The antioxidant activity of a compound can be assayed by its ability to scavenge the superoxide ($O_2^{\cdot -}$) produced by the xanthine−xanthine oxidase reaction (Scheme 1). This is manifested as an inhibition in the rate of production of formazan.[30−32]

The antioxidative efficacies of PV, PR, BPR, CAS, and ECR are shown in Table 2 (also see Supporting Information). To know whether there was any alteration in $O_2^{\cdot -}$ generation in the reaction due to enzyme (xanthine oxidase) inhibition following the addition of different analogues, the production of uric acid was monitored. The observations revealed that there was no marked change in $O_2^{\cdot -}$ generation because the production of uric acid in all of the reactions was almost the same and in the range of only ±3.0%. The antioxidant activity order for the analogues is BPR > PR > PV > ECR, CAS, which is the same as that obtained by the EMSA and the formation-constant studies. This provides additional support for investigating the NF-κB inhibitory activity of these analogues.

Conclusions

The discovery of the role of NF-κB in the regulation of HIV-1 gene expression has stimulated an intensive search for the inhibitors of NF-κB. Our group is working on the design of new NF-κB-DNA binding inhibitors.[18,21,22] Recently, we reported that ATA is a potent NF-κB-DNA binding inhibitor.

Work on other ATA analogues against NF-κB has not been previously reported. For this purpose, we have studied this class with the aim of establishing structure−activity relationships. On the basis of the results presented earlier, the following structural design requirements for ATA analogues to act as NF-κB-DNA binding inhibitors are proposed. The inactivity of AU and FL indicate that the presence of a chelating site on the analogue is essential for NF-κB-DNA binding inhibitory activity. A comparison of active and inactive analogues reveals that the minimal structural requirements for inhibitory activity in the series includes catechol function or salicylic acid function in two of the three aromatic nuclei and a sulfonic or carboxylic acid group in the third aromatic ring. A comparison of ATA, CAS, and ECR shows that the presence of a methyl group ortho to salicylic acid configuration leads to loss in inhibitory activity. The presence of halogen groups on the rings containing catechol

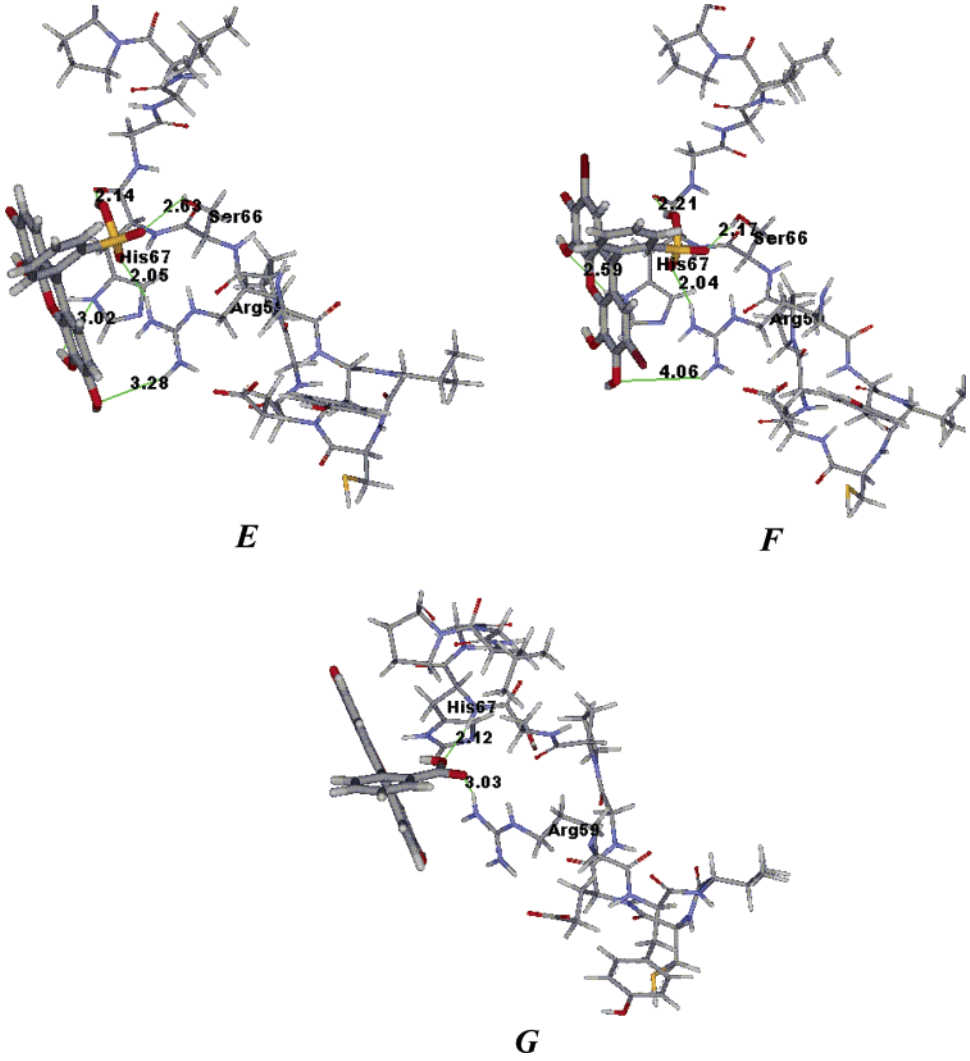

Figure 9. Possible binding modes of the ATA analogues with the p50 DNA binding region. E−G represent the complexes with analogues PR, BPR, and FL, respectively. The hydrogen bonds are depicted as green lines, and the distances are in Å.

Scheme 1

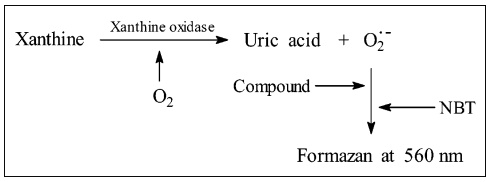

Table 2. Superoxide Scavenging Activities of the ATA Analogues

ATA analogue	IC_{50} (μM)
pyrocatechol violet	120.0
pyrogallol red	88.0
bromopyrogallol red	51.5
chrome azurol S	>250.0
eriochrome cyanine R	>250.0

(BPR) and the presence of an ether linkage between these rings (BPR, PR) increases inhibitory activity.

Experimental Section

ATA analogues used in these experiments were purchased from commercial sources. PV, PR, and BPR were supplied by Acros Organics. CAS was purchased from Aldrich, ECR from Central Drug House, and Fluorescein and Aurin from TCI, Tokyo.

GST-p50 Bacterial Protein Preparation. In GST-p50, the FspI-ApaI fragment of p105 NF-κB cDNA, which covers the first 464 amino acids, was inserted into pGEX. *Escherichia coli* strain BL21 was transformed with each plasmid, and GST fusion proteins were purified using glutathione-sepharose column chromatography as described previously by Inoue et al.[33,34]

Electrophoretic Mobility Shift Assay (EMSA). A biotinated double-stranded oligonucleotide containing a κB site from the mouse immunoglobulin κ light chain enhancer

5′-Biotin-AGCTTCAGAGGGGACTTTCCGAGAGG-3′

3′-AGTCTCCCCTGAAAGGCTCTCCAGCT-Biotin-5′

was used. Purified GST-p50 (5 ng) was used for the EMSA. After the incubation of each reaction mixture containing the binding buffer (15 mM Tris-HCl (pH 7.5), 75 mM NaCl, 1.5 mM EDTA, 1.5 mM dithiothreitol, 7.5% glycerol, 0.3% NP-40, 1 mg/mL BSA), 0.5 μg of polydI-dC, GST-p50 , and each analogue at room temperature for 5 min, the labeled DNA probe (30 000 cpm) was added, and the mixture was further incubated at room temperature for 20 min. The sample in a volume of 10 μL was loaded onto 4% poly(acrylamide) gels and electrophoresed at 80 CV. After this, the gel was transferred to a nylon membrane. The biotin end-labeled DNA was detected using the streptavidin-horseradish peroxidase conjugate and lightshift chemiluminescent substrate.[35] This chemiluminescence assay method offers the sensitivity and speed of radioactive assays without the hazards, waste, and probe-instability problems associated with radioactive systems.

Chemical Speciation and Formation-Constant Studies of the Zn^{2+}−ATA Analogue Complex. The pH-metric technique is a robust and versatile way of measuring the ionization and distribution of drugs in biological fluids and assessing their interaction with

trace metal ions. pH-metric titration has been carried out with the digital pH meter ELICO LI 120 with a combined glass electrode. The glass electrode was calibrated before the titrations as described by Martell and Motekaitis.[27] To ensure constant ionic strength (0.1 M) during the titrations, an electrolyte, sodium perchlorate $NaClO_4$, was added in requisite amounts. A solution of tetramethylammonium hydroxide (TMAH) (E. Merck) was used as the titrant. The zinc ion solution was prepared from Analar (BDH) samples of the zinc sulfate and was standardized by the conventional methods described by Vogel.[36]

The titrations were performed in a covered glass jacketed titration cell under a stream of presaturated nitrogen. Measurements for BPR and PR were made in a 12.5% ethanol/water medium at 25 °C (± 0.5 °C), maintained constant by using a Julabo VC type thermostat. For PV, CAS, and ECR, the measurements were made in an aqueous medium at 25 °C (± 0.5 °C). Stepwise dissociation constants within the range of the potentiometric titrations (up to pH 12.0) were calculated. Formation constants of the complexes were determined by direct potentiometric titration using Bjerrum's method[25] as modified by Irving and Rossotti[26] and the weighted least-squares technique. The program SPE[27] was used for drawing the species distribution curve.

Molecular Modeling. Docking Studies. The 3D structure of NF-κB (p50), obtained from the Protein Data Bank (pdb id: 1NFK)[37] was used to dock the analogues. Docking studies were performed with the GOLD 2.0 program,[38] and the details of the docking procedure have been described in detail in our previous studies.[28] Briefly, the amino acid residues 59−71 (the DBR) in p50, which have been described to be very important in κB site specific DNA recognition,[10] were defined as the docking site. Docking simulations were performed in standard default settings to get the best predictive accuracy. GoldScore was used to rank the relative docking energies, and the highest scored solutions were considered. GoldScore[39] is a fitness function implemented in the GOLD program, which has four components: (a) protein−ligand hydrogen bond energy, (b) protein−ligand van der Waals energy, (c) ligand intramolecular hydrogen bond energy, and (d) ligand internal van der Waals energy. The Insight II molecular modeling package[40] was used for further analyses of the docked complexes.

Parametrization and Energy Refinement of Complexes. All of the complexes were refined in the presence of explicit solvent, with a progressive energy-minimization protocol using the AMBER force field.[41] First, all of the complexes were solvated by an 8 Å thick shell of pre-equilibrated TIP3P water molecules. Next, in a progressive minimization protocol, first, the hydrogens of the system were minimized, and next, only the water molecules were allowed to minimize so as to let them adapt in the electric field of the complex. This was followed by a minimization of the side chains and then the inhibitor. Finally, all of the system was minimized while keeping the C_α-trace backbone atoms of the protein restrained to their crystallographic position with a force constant of 32 kcal mol^{-1} $Å^{-2}$. This approach allowed us to gradually refine the complexes while not introducing artifacts of excessive minimization on the high-resolution backbone structure of the protein. All of the minimizations included 1000 steps of steepest descent followed by 5000 steps of conjugate-gradient energy minimization, until the root-mean-square value of the potential energy gradient was <0.01 kcal mol^{-1} $Å^{-1}$. A nonbonded cutoff of 10 Å was used throughout. The partial charges for the inhibitors were derived from a RESP (restrained electrostatic potential) fitting procedure[42] at a 6-31G* level. Single point, gas-phase calculations on the inhibitors at the 6-31G* level were performed using the Gaussian quantum-chemistry package.[43] Parameters for angles, bonds, and torsions were taken either from energy-minimum structures or derived by analogy, on the basis of existing parameters.

Molecular Electrostatic Potentials. To understand the molecular recognition between the inhibitors and p50-DBR from an electrostatic point of view, MEP maps were generated for each inhibitor. First, the geometries of all of the inhibitors (built in Insight II) were energy minimized with an ab initio method, using the B3LYP functional and 3-21G(d) basis set. Next, single-point calculations (performed at 6-31G* level), as described in the above section, were used to map the net electron density around each inhibitor. MOLEKEL 4.3[44] was used to map the electrostatic potential onto the electron density surface.

Antioxidant Activity. Assay for Superoxide Anion Generation. The superoxide generation assay[30,31] was performed with a little modification in the method adopted elsewhere.[32] The typical reaction mixture in a total volume of 1.0 mL contained phosphate buffer (0.1 M, pH 7.4), l-methionine (10 mM), nitroblue tetrazolium (NBT) (57.0 mM), and xanthine (1.0 mM). The reaction mixture was incubated for 5 min at room temperature (25 ± 2 °C). The reaction was initiated by the addition of 50 milliunits of xanthine oxidase. Superoxide production was spectrophotometrically evaluated (SL 159, ELICO spectrophotometer) by monitoring the reduction of NBT to formazan at 560 nm.

Assay for Superoxide Anion Scavenging by Compounds. Five concentrations, 50, 100, 150, 200 and 250 μM, of the analogues, pyrocatechol violet, pyrogallol red, bromopyrogallol red, chrome azurol S, and eriochrome cyanine R, were added in the reaction mixture for the assay of $O_2^{\cdot -}$ generation described above while testing antioxidative efficacy. The kinetics of the reaction was followed in two sets, that is, the controls and by adding different compounds. The percentage inhibition in formazan formation was recorded because of the increase in the scavenging of $O_2^{\cdot -}$ in the latter set comparing the controls.

In the above reaction, the product is uric acid (trihydroxy purine) formed as a catabolism of xanthine (dihydroxy purine), reacted upon by xanthine oxidase. The production of uric acid was also spectrophotometrically measured at 290 nm[45] in controls as well as by adding the compounds. These experiments were conducted to workout if there were some alterations in $O_2^{\cdot -}$ generation due to the enzyme inhibition by the studied compounds.

Acknowledgment. M.J.R. would like to thank NFCR Center for Computational Drug Discovery, University of Oxford, U.K. for a doctoral scholarship to V.P. and Fundação para a Ciência e Tecnologia, Portugal for financial support. R.K.S. thanks JSPS (Japan) and CSIR (India) for financial assistance.

Supporting Information Available: Energy-minimized structures of the ATA analogues, molecular electrostatic potentials of the energy minimized structures of ATA analogues, and antioxidant efficacies of the ATA analogues. The material is available free of charge via the Internet at http://pubs.acs.org.

References

(1) De Clercq, E. In *Antiviral Agents and Human Viral Diseases*; Galasso, G. J., Whitley, R. J., Merigan, T. C., Eds.; Lippincott-Raven: Philadelphia, PA 1997; p 1.
(2) Ghosh, S.; May, M. J.; Kopp, E. B. NF-kappa B and Rel proteins: evolutionarily conserved mediators of immune responses. *Annu. Rev. Immunol.* **1998**, *16*, 225−260.
(3) Baldwin, A. S., Jr. The NF-kappa B and I kappa B proteins: new discoveries and insights. *Annu. Rev. Immunol.* **1996**, *14*, 649−683.
(4) Israel, A. The IKK complex: an integrator of all signals that activate NF-kappaB. *Trends Cell. Biol.* **2000**, *10*, 129−133.
(5) Siebenlist, U.; Franzoso, G.; Brown, K. Structure, regulation and function of NF-kappa B. *Annu. Rev. Cell Biol.* **1994**, *10*, 405−455.
(6) Baeurle, P. A.; Henkel, T. Function and activation of NF-kappa B in the immune system. *Annu. Rev. Immunol.* **1994**, *12*, 141−179.
(7) Anderson, K. V. Toll signaling pathways in the innate immune response. *Curr. Opin. Immunol.* **2000**, *12*, 13−19.
(8) Chen-Park, F. E.; Huang, D.-B.; Noro, B.; Thanos, D.; Ghosh, G. The κB DNA sequence from the HIV long terminal repeat functions as an allosteric regulator of HIV transcription. *J. Biol. Chem.* **2002**, *277*, 24701−24708.
(9) Phelps, C. B.; Sengchanthalangsy, L. L.; Malek, S.; Ghosh, G. Mechanism of kappa B DNA binding by Rel/NF-kappa B dimers. *J. Biol. Chem.* **2000**, *275*, 24392−24399.
(10) Berkowitz, B.; Huang, D.-B.; Chen-Park, F. E.; Sigler, P. B.; Ghosh, G. The X-ray crystal structure of the NF-κB p50-p65 heterodimer bound to the interferon $\beta-\kappa$B site. *J. Biol. Chem.* **2002**, *277*, 24694−24700.

(11) Hiscott, J.; Kwon, H.; Genin, P. Hostile takeovers: viral appropriation of the NF-kappaB pathway. *J. Clin. Invest.* **2001**, *107*, 143−151.
(12) Dickinson, L. A.; Trauger, J. W.; Baird, E. E.; Dervan, P. B.; Graves, B. J.; Gottesfeld, J. M. Inhibition of Ets-1 DNA binding and ternary complex formation between Ets-1, NF-kappaB, and DNA by a designed DNA-binding ligand. *J. Biol. Chem.* **1999**, *274*, 12765−12773.
(13) Chen, F. E.; Huang, D.-B.; Chen, Y. Q.; Ghosh, G. Crystal structure of p50/p65 heterodimer of transcription factor NF-kappaB bound to DNA. *Nature* **1998**, *391*, 410−413.
(14) Muller, C. W.; Rey, F. A.; Sodeoka, M.; Verdine, G. L.; Harrison, S. C. Structure of the NF-kappa B p50 homodimer bound to DNA. *Nature* **1995**, *373*, 311−317.
(15) Nabel, G.; Baltimore, D. An inducible transcription factor activates expression of human immunodeficiency virus in T cells. *Nature* **1987**, *326*, 711−713.
(16) Ensoli, B.; Barillari, G.; Salahuddin, S. Z.; Gallo, R. C.; Wong-Staal, F. Tat protein of HIV-1 stimulates growth of cells derived from Kaposi's sarcoma lesions of AIDS patients. *Nature* **1990**, *345*, 84−86.
(17) Pande, V.; Ramos, M. J. Nuclear Factor Kappa B: A potential target for anti-HIV chemotherapy. *Curr. Med. Chem.* **2003**, *10*, 1603−1615.
(18) Sharma, R. K.; Otsuka, M.; Pande, V.; Inoue, J.-i.; Ramos, M. J. Evans Blue is an inhibitor of nuclear factor-kappa B (NF-kappaB)-DNA binding. *Bioorg. Med. Chem. Lett.* **2004**, *14*, 6123−6127.
(19) Zabel, U.; Schreck, R.; Baeuerle, P. A. DNA binding of purified transcription factor NF-κB. *J. Biol. Chem.* **1991**, *266*, 252−260.
(20) Otsuka, M.; Fujita, M.; Aoki, T.; Ishii, T.; Sugiura, Y.; Yamamoto, T.; Inoue, J.-i. Novel zinc chelators with dual activity in the inhibition of the κB site-binding proteins HIV-EP1 and NF-κB. *J. Med. Chem.* **1995**, *38*, 3264−3270.
(21) Sharma, R. K.; Pande, V.; Ramos, M. J.; Rajor, H. K.; Chopra, S.; Meguro, K.; Inoue, J.-i. Inhibitory activity of polyhydroxycarboxylate chelators against recombinant NF-κB p50 protein-DNA binding. *Bioorg. Chem.* **2005,** *33*, 67−81.
(22) Sharma, R. K.; Garg, B. S.; Kurosaki, H.; Goto, M.; Otsuka, M.; Yamamoto, T.; Inoue, J.-i. Aurine tricarboxylic acid, a potent metal-chelating inhibitor of NFκB-DNA binding. *Bioorg. Med. Chem.* **2000**, *8*, 1819−1823.
(23) Berg, J. M.; Shi, Y. The galvanization of biology: a growing appreciation for the roles of zinc. *Science* **1996**, *271*, 1081−1085.
(24) Prasad, A. S.; Bao, B.; Beck, F. W. J.; Sarkar, F. H. Zinc activates NF-κB in HUT-78 cells. *J. Lab. Clin. Med.* **2001**, *138*, 250−256.
(25) Bjerrum, J. Metal Amine Formation in Aqueous Solutions. Theory of reversible step reactions; P. Haase and Son: Copenhagen, 1941.
(26) Irving, H. M.; Rossotti, H. S. The calculation of formation curves of metal complexes from pH titration curves in mixed solvents. *J. Chem. Soc.* **1954**, 2904−2910.
(27) Motekaitis, R. J.; Martell, A. E. *The Determination and Use of Stability Constants*, 2nd ed.; VCH Publishers, Inc.: New York, 1992.
(28) Pande, V.; Sharma, R. K.; Inoue, J.-i.; Otsuka, M.; Ramos, M. J. A molecular modeling study of inhibitors of nuclear factor kappa-B (p50)-DNA binding. *J. Comput.-Aided Mol. Des.* **2003**, *17*, 825−836.
(29) Murray, J. S.; Politzer, P., In Schleyer, P. V. R.; Allinger, N. L.; Clark, T.; Gasteiger, J.; Kollman, P. A.; Schaefer, H. F., III, Schreimer, P. R., Eds.; *The Encyclopedia of Computational Chemistry*; Wiley and Sons: Chichester, U.K. 1997.
(30) Sharma, S. D.; Rajor, H. K.; Chopra, S.; Sharma, R. K. Studies on structure activity relationship of some dihydroxy-4-methylcoumarin antioxidants based on their interaction with Fe(III) and ADP. *BioMetals* **2005**, *18*, 143−154.
(31) Athar, M.; Sharma, S. D.; Iqbal, M.; Sultana, S.; Pandeya, K. B.; Tripathi, I. P. Coordination of copperpolyamine complex with imidazoles potentiates its superoxide dismutase mimicking activity and abolishes its interaction with albumin. *Biochem. Mol. Biol. Int.* **1996**, *39*, 813−821.
(32) Darr, D.; Zarilla, K. A.; Fridovich, I. A mimic of superoxide dismutase activity based upon desferrioxamine B and manganese-(IV). *Arch. Biochem. Biophys.* **1987**, *258*, 351−355.
(33) Inoue, J.; Kerr, L. D.; Kakizuka, A.; Verma, I. M. I kappa B gamma, a 70 kd protein identical to the C-terminal half of p110 NF-kappa B: a new member of the I kappa B family. *Cell* **1992**, *68*, 1109−1120.
(34) Inoue, J.; Takahara, T.; Akizawa, T.; Hino, O. Bcl-3, a member of the I kappa B proteins, has distinct specificity towards the Rel family of proteins. *Oncogene* **1993**, *8*, 2067−2073.
(35) Pierce Biotechnology, Inc., Rockford, IL.
(36) Vogel, V. A. *Text Book of Quantitative Inorganic Analysis*, 4th ed.; Longmans, ELBS: New York, 1978.
(37) Ghosh, G.; Van Duyne, G.; Ghosh, S.; Sigler, P. B. Structure of NF-kappa B p50 homodimer bound to a kappa B site. *Nature* **1995**, *373*, 303−310.
(38) *GOLD 2.0*, CCDC software Ltd.: Cambridge, U.K.
(39) Jones, G.; Willett, P.; Glen, R. C.; Leach, A. R.; Taylor, R. Development and validation of a genetic algorithm for flexible docking. *J. Mol. Biol.* **1997**, *267*, 727−748.
(40) *INSIGHT II*, Accelrys Inc.: San Diego, CA.
(41) Case, D. A.; Darden, T. A.; Cheatham, T. E., III; Simmerling, C. L.; Wang, J.; Duke, R. E.; Luo, R.; Merz, K. M.; Wang, B.; Pearlman, D. A.; Crowley, M.; Brozell, S.; Tsui, V.; Gohlke, H.; Mongan, J.; Hornak, V.; Cui, G.; Beroza, P.; Schafmeister, C.; Caldwell, J. W.; Ross, W. S.; Kollman, P. A. *AMBER 8*; University of California: San Francisco, CA, 2004.
(42) Bayly, C. I.; Cieplak, P.; Cornell, W. D.; Kollman, P. A. A well-behaved electrostatic potential based method using charge restraints for deriving atomic charges: the RESP model. *J. Phys. Chem.* **1993**, *97*, 10269−10280.
(43) Frisch, M. J.; Trucks, G. W.; Schlegel, H. B.; Scuseria, G. E.; Robb, M. A.; Cheeseman, J. R.; Montgomery, J. A., Jr.; Vreven, T.; Kudin, K. N.; Burant, J. C.; Millam, J. M.; Iyengar, S. S.; Tomasi, J.; Barone, V.; Mennucci, B.; Cossi, M.; Scalmani, G.; Rega, N.; Petersson, G. A.; Nakatsuji, H.; Hada, M.; Ehara, M.; Toyota, K.; Fukuda, R.; Hasegawa, J.; Ishida, M.; Nakajima, T.; Honda, Y.; Kitao, O.; Nakai, H.; Klene, M.; Li, X.; Knox, J. E.; Hratchian, H. P.; Cross, J. B.; Bakken, V.; Adamo, C.; Jaramillo, J.; Gomperts, R.; Stratmann, R. E.; Yazyev, O.; Austin, A. J.; Cammi, R.; Pomelli, C.; Ochterski, J. W.; Ayala, P. Y.; Morokuma, K.; Voth, G. A.; Salvador, P.; Dannenberg, J. J.; Zakrzewski, V. G.; Dapprich, S.; Daniels, A. D.; Strain, M. C.; Farkas, O.; Malick, D. K.; Rabuck, A. D.; Raghavachari, K.; Foresman, J. B.; Ortiz, J. V.; Cui, Q.; Baboul, A. G.; Clifford, S.; Cioslowski, J.; Stefanov, B. B.; Liu, G.; Liashenko, A.; Piskorz, P.; Komaromi, I.; Martin, R. L.; Fox, D. J.; Keith, T.; Al-Laham, M. A.; Peng, C. Y.; Nanayakkara, A.; Challacombe, M.; Gill, P. M. W.; Johnson, B.; Chen, W.; Wong, M. W.; Gonzalez, C.; Pople, J. A. *Gaussian 03*, revision A1; Gaussian, Inc.: Wallingford, CT, 2004.
(44) Portmann, S.; Luthi, H. P. Molekel: an interactive molecular graphics tool. *Chimia* **2000**, *54*, 766−769.
(45) Pasternack, R. F.; Halliwell, B. Superoxide dismutase activities of an iron porphyrin and other iron complexes. *J. Am. Chem. Soc.* **1979**, *101*, 1026−1031.

JM050617X